

Understanding the Reaction Steps Involving Polysulfides in 1 M LiTFSI in TEGDME:DOL Using Cyclic Voltammetry Experiments and Modelling

Vigneshwaran Thangavel,^[a, b] Afef Mastouri,^[a, b, c] Claude Guéry,^[a, b, c] Mathieu Morcrette,^[a, b, c] and Alejandro A. Franco^{*[a, b, c, d]}

The reaction mechanisms of polysulfides in the electrolytes of lithium sulfur (Li–S) batteries are known to be complex. These reaction mechanisms may also change with the electrolyte used. Understanding the reaction steps of the polysulfides in a Li–S battery electrolyte is important to assess the underlying phenomena behind the Li–S cell performance limitations. Here, we investigate the reaction steps of polysulfides in electrolyte solutions containing S_8 , Li_2S_8 and Li_2S_6 in 1 M LiTFSI in TEGDME:DOL (v/v 1:1) (one of the most interesting electrolytes

for use in Li–S batteries), using experimental cyclic voltammetry and a mathematical model. The mathematical model assists in understanding the reaction steps behind the characteristics changes of cyclic voltammograms (CVs) with the scan rate and polysulfides speciation. Our systematic study shows that the reaction steps conventionally used in Li–S battery models are not sufficient to simulate all the CV characteristics of the investigated electrolyte solutions.

1. Introduction

Lithium sulfur (Li–S) batteries have the potential to deliver up to two to three times the energy density of lithium ion batteries (LIBs).^[1] This is chiefly due to the superior gravimetric specific capacity of carbon/sulfur cathodes in Li–S batteries. The active material of the Li–S batteries cathode is sulfur (S), whose molar mass is lower than those of the transition metal oxides used in LIBs. Furthermore, each mole of S could accept up to two moles of electrons and lithium ions (Li^{+}). During discharge, the conversion of initial $S_{8(s)}$ to final $Li_2S_{(s)}$ occurs through a series of intermediate reactions steps involving polysulfides dissolved in the electrolyte.^[2] The polysulfides are produced via the dissolution of $S_{8(s)}$ and the subsequent reduction of dissolved

sulfur (S_8) in the electrolyte. The presence of different polysulfide intermediates and their reaction steps change with the solvents used in the electrolyte.^[3–5] Therefore identifying all the possible polysulfides in the electrolyte and their reaction steps can assist in improving the assessment of performance limitations. Spectroscopic techniques assist in estimating the evolutions of dissolved polysulfides in the Li–S battery electrolytes, based on which their reaction steps are hypothesized.^[3,6–8] However, combined experimental and modelling based electrochemical studies are required to verify the hypothesized reaction steps of polysulfides in the electrolytes.

Cyclic voltammetry is an electrochemical potential sweep technique and it has been extensively used to analyze the dissolved polysulfides in nonaqueous electrolytes for several decades.^[3,9–14] Cyclic voltammograms (CVs) of dissolved sulfur (S_8) in nonaqueous organic electrolytes, have long been known to possess two distinctive reduction peaks and sometimes with a small intermediate peak termed *prewave* in between them which is observed in some electrolytes.^[9,12,13,15,16] However, CV of S_8 in 1 M lithium bis(trifluoromethanesulfonyl)imide (LiTFSI) in dioxane:dimethoxyethane (Diox:DME) consists only one reduction peak.^[5] While, the number of oxidation peaks vary from one to three based on the solvents used in the electrolyte solutions.^[5]

Due to these significant characteristics variations, CVs of dissolved S_8 in different electrolytes were used to compare the impact of solvent properties such as donor number,^[3] acceptor number and dielectric constant, on the existence and reaction mechanisms of polysulfides.^[5] The changes in the CV characteristics in different electrolytes is correlated to the changes in the galvanostatic curves such as the separation of discharge plateaus, charge/discharge polarization among others.^[3,5] Furthermore, the characteristics variations of CVs with the

- [a] Dr. V. Thangavel, Dr. A. Mastouri, Prof. Dr. C. Guéry, Dr. M. Morcrette, Prof. Dr. A. A. Franco
Laboratoire de Réactivité et Chimie des Solides (LRCS),
UMR CNRS 7314
Université de Picardie Jules Verne,
Hub de l'Energie
15 Rue Baudelocque, 80039 Amiens Cedex, France
E-mail: alejandro.franco@u-picardie.fr
 - [b] Dr. V. Thangavel, Dr. A. Mastouri, Prof. Dr. C. Guéry, Dr. M. Morcrette, Prof. Dr. A. A. Franco
Réseau sur le Stockage Electrochimique de l'Energie (RS2E),
FR CNRS 3459
Hub de l'Energie
15 Rue Baudelocque, 80039 Amiens Cedex, France
 - [c] Dr. A. Mastouri, Prof. Dr. C. Guéry, Dr. M. Morcrette, Prof. Dr. A. A. Franco
ALISTORE-ERI, European Research Institute,
FR CNRS 3104
Hub de l'Energie
15 Rue Baudelocque, 80039 Amiens Cedex, France
 - [d] Prof. Dr. A. A. Franco
Institut Universitaire de France
103 Boulevard Saint Michel, 75005 Paris, France
-  Supporting information for this article is available on the WWW under <https://doi.org/10.1002/batt.202000175>

operation conditions in some electrolytes were also used to deduce the reaction mechanisms of S_8 and polysulfides.

Yamin *et al.* studied the cyclic voltammetry of different polysulfides dissolved in 1 M Lithium perchlorate (LiClO_4) in Tetrahydrofuran (THF), where they compared the impact of polysulfide chain lengths, concentrations and scan rate on the peak currents in order to deduce the kinetics and plausible reaction mechanism.^[17] Cyclic voltammetry was also used to quantify the crossover of polysulfides through ion-selective membranes, in order to assess their effectiveness in limiting polysulfide shuttle.^[18,19] A recent review by Haung *et al.* discusses in detail the challenges and opportunities of cyclic voltammetry in Li–S batteries.^[20]

Few of the previous cyclic voltammetry studies of dissolved S_8 and lithium polysulfides have utilized mathematical models to simulate the experimental CVs and to interpret the underlying reaction mechanisms behind them. Levillain *et al.* and Jung *et al.* have proposed mathematical models to simulate the first reduction and oxidation peaks of S_8 dissolved in Dimethylformamide (DMF), which are based on reaction mechanisms involving two common one-electron electrochemical reactions namely S_8/S_8^{*-} and S_8^{*-}/S_8^{2-} .^[15,21] Gaillard *et al.*, investigated the half CV (1st oxidation and reduction peaks are not considered) of Li_2S_6 in DMF to identify the reaction mechanism behind their peaks using spectroelectrochemical measurements. They proposed a cyclic voltammetry model which considers S_4^{*-} and S_3^{*-} as the only reducible polysulfides that produce S_4^{2-} and S_3^{2-} respectively, which could then be reoxidized.^[22] Levillain *et al.*, also studied the half CV of Li_2S_6 in liquid ammonia (NH_3) and they were the first to distinguish the peaks corresponding to the reductions of S_3^{*-} and S_6^{2-} which produce S_3^{2-} and S_6^{3-} , respectively.^[23] Recently Mačák *et al.*, reported a numerical investigation of Li–S batteries using a cyclic voltammetry model in which the porous electrode is simplified to a single particle or a planar electrode.^[24] However, this model utilizes a conventionally assumed reaction mechanism for simulating CVs.

It is clear from the above examples, that there are several reported studies devoted to the investigation of the impacts of different electrolytes on the CV characteristics of dissolved S_8 . However, there are very few comparative cyclic voltammetry studies of different types of lithium polysulfides and S_8 dissolved in a single electrolyte which assist in understanding the reaction steps as suggested by Yamin *et al.*^[17] Therefore, this paper presents a comparative cyclic voltammetric study of different polysulfides solutions such as S_8 , Li_2S_8 and Li_2S_6 dissolved in 1 M LiTFSI in tetraethylene glycol dimethyl ether: dioxolane (TEGDME:DOL), which is one of the widely used Li–S battery electrolytes. Although DME:DOL is the most widely used solvent mixture in Li–S batteries, TEGDME:DOL is particularly attractive for commercial use due to its safety. DME has a very low flash point,^[25] therefore the electrolyte becomes highly flammable when it is used.^[26] On the contrary, TEGDME has a very high flash point,^[27] therefore it is much safer to use. Therefore, we chose 1 M LiTFSI in TEGDME:DOL as our model electrolyte.

In this paper, a mathematical model is used to simulate and interpret the experimental CVs. The objective of this paper is to

assess the reaction steps of the dissolved polysulfides that correspond to certain CV characteristics and their variation with the operating conditions such as the dissolved polysulfides speciation and scan rates. Here we report the complete simulated CVs *i.e.* both reduction and oxidation of different electrolyte solutions containing S_8 , Li_2S_8 and Li_2S_6 in 1 M LiTFSI in TEGDME:DOL. Furthermore, our model is able to simulate the variations of CV characteristics with the cycle number. All these simulations were carried out using a single set of parameters values. Through this procedure, we have attempted to determine the reaction mechanism of the dissolved polysulfides in 1 M LiTFSI in TEGDME:DOL.

Experimental Section

Cell setup

A relatively simple three-electrode cell setup was used to carry out cyclic voltammetric measurements of sulfur and polysulfides in 1 M LiTFSI in TEGDME:DOL (1:1) contained in a glass beaker (Figure 1). A glassy carbon electrode with diameter 1.6 mm was used as the working electrode and a Platinum (Pt) grid was used as the counter electrode.^[28] It should be known that most of the previously reported cyclic voltammetric studies of dissolved S_8 and polysulfides were carried out using planar working electrodes like glassy carbon,^[5,13,15,29–31] since it is considered to be a well behaved electrode.^[32] Furthermore, the porous carbon working electrode was not used in this study – since it introduces complexities such as anisotropic distribution of species concentrations, additional physics and parameters for modelling, etc. which would impede the proper understanding of the polysulfides reaction mechanism in the electrolyte. Silver/Silver nitrate (Ag/AgNO_3) electrode was used as the reference electrode, which consists of an Ag wire immersed in a solution containing 10 mM of AgNO_3 and 0.1 M of Tetrabutylammonium perchlorate (TBAP) in acetonitrile contained in a glass tube fitted with a frit at its extremity. Since the reference and working electrolytes are different in our experiment, a liquid junction potential difference (LJP) could exist between them. However, this LJP and the overall potential of our Ag/AgNO_3 reference electrode could be assumed to remain stable, since the frit restricts the diffusion of species across it and prevents the leakage of the reference electrolyte into the ones under investigation in this work.

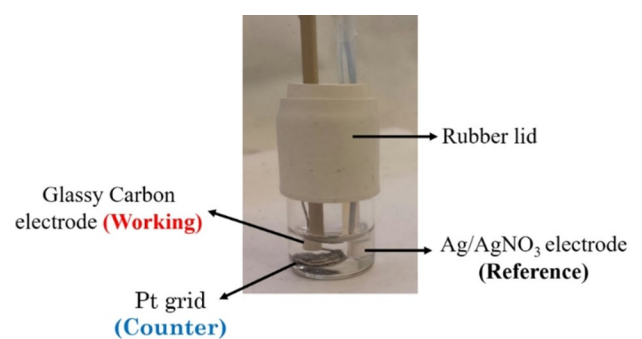


Figure 1. Three-electrode cell setup used in our CV studies.

Preparation of the Electrolyte Solutions Containing the Polysulfides

S_8 was dissolved in the electrolyte to a concentration of 6 mM, which is measured to be its solubility. In practical Li-S batteries, polysulfides can reach high concentrations, however the solubility of different polysulfides in 1 M LiTFSI in TEGDME:DOL are not known experimentally. Since the objective of this work is to understand the reaction mechanism of dissolved polysulfides in the electrolyte, the use of high polysulfides concentrations was avoided to prevent precipitation reactions. Therefore, the polysulfides containing solutions were prepared by stirring stoichiometric quantities of Li_2S and S_8 amounting to a standard concentration of 50 mM of Li_2S_x in 5 ml of 1 M LiTFSI in TEGDME:DOL (1:1).^[28] The preparation was carried out inside the glove box under Ar atmosphere for 5 days with temperature maintained between 25–27 °C. Followed by 3 days of decantation process, 1.5 mL of the resulting supernatant solutions were extracted and used for the cyclic voltammetry measurements.

Cyclic Voltammetry Measurements

The entire cell setup was assembled inside a glove box under Ar atmosphere and sealed using a rubber lid. Cyclic voltammetry measurements were done outside the glove box using Biologic VMP3 with the temperature maintained at 25 °C. The potential between the working and reference electrodes was swiped, starting from and ending at an open circuit potential (OCV) after reaching a minimum value during the scan towards negative direction and a maximum value for the scan towards positive direction, thereby constituting a cycle.

2. Theoretical Methodology

2.1. Simulated Domain and Governing Equations

Since our experiments were carried out using a three electrode cell setup (Figure 1), the measured current signals correspond to the electrochemical reactions that occur at the working electrode/electrolyte interface. Therefore, the simulation domain consists only the diffusion layer (DL) at the vicinity of the working electrode (Figure 2) whose thickness is given by Equation (1)^[33]

$$\delta_{DL} = 6\sqrt{D_{max}t_{max}} \quad (1)$$

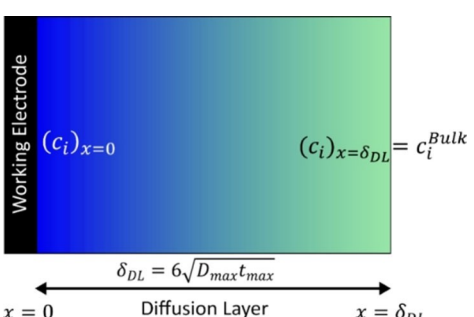


Figure 2. Schematic representation of the simulated domain.

where D_{max} is the diffusion coefficient of the species which has the fastest diffusivity (Table 4) and t_{max} is the total duration of the experimental cyclic voltammetry measurement.

Since the working glassy carbon electrode is flat and planar, the diffusion fields of different species in the DL will have points that are equivalent at a given distance (x) from the electrode surface.^[33] Therefore, the net flux of species will occur perpendicular to the electrode surface along the thickness of the DL and the spatiotemporal distribution of a species (i) concentration can be suitably described by a one-dimensional mass conservation equation, as follows [Eq. (2)]

$$\frac{\partial c_i}{\partial t} = \frac{\partial}{\partial x} \left(D_i \frac{\partial c_i}{\partial x} \right) - s_i - G_i \quad (2)$$

where c_i and D_i are the concentration and diffusion coefficient of the species i , while s_i and G_i respectively are its sink/source terms brought about by some homogeneous chemical and heterogeneous dissolution/precipitation reactions

$$s_i = \sum_j \vartheta_{ij} k_j^f \left(\prod_i ((c_i)^{\vartheta_{ij}})_{\vartheta_{ij}>0} - K_j^{eq} \prod_i ((c_i)^{-\vartheta_{ij}})_{\vartheta_{ij}<0} \right) \quad (3)$$

In the Equation (3), ϑ_{ij} is the stoichiometric coefficient for the species i involved in the homogenous chemical reaction j [Eq. (23) or (25)]. k_j^f and k_j^r are forward and reverse kinetic constants. K_j^{eq} is the equilibrium constant of the chemical reaction j , which is given by Equation (4)

$$K_j^{eq} = \frac{k_j^r}{k_j^f} \quad (4)$$

The bulk concentrations of all the species (c_i^*) are assumed to remain constant and the concentrations of species at the boundary $x = \delta_{DL}$ are equal to those of the bulk [Eq. (5)]

$$(c_i)_{x=\delta_{DL}} = c_i^* \quad (5)$$

while the flux of a species (N_i) at the electrode surface ($x = 0$) is given by the Faraday's law [Eq. (6)]

$$(N_i)_{x=0} = \left(D_i \frac{\partial c_i}{\partial x} \right)_{x=0} = \frac{A}{A^0} \sum_j \frac{S_{ij} i_j}{n_j F} \quad (6)$$

In the equation above, A [calculated using Eq. (10)] and A^0 are the electro-active and the geometrical surface areas of the flat working electrode, respectively. S_{ij} , n_j and i_j are respectively the stoichiometric coefficient of the species i (see Supporting Information), number of electrons and current density of an electrochemical reaction j of form [Eq. (7)],

$$\sum_i S_{ij} M_i^{z_i} = n_j e^- \quad (7)$$

where $M_i^{z_i}$ and e^- respectively represent a species i and an electron. z_i is the charge of the species i .

The current density of an individual electrochemical reaction is given by the Butler-Volmer equation [Eq. (8)],

$$i_j = i_j^0 \left(\prod_i \left((c_i)_{x=0}^{S_{ij}} \right)_{S_{ij}>0} e^{\left(\frac{(1-\alpha_j)n_F(E-U_j^0)}{RT} \right)} - \prod_i \left((c_i)_{x=0}^{-S_{ij}} \right)_{S_{ij}<0} e^{\left(\frac{-\alpha_j n_F(E-U_j^0)}{RT} \right)} \right) \quad (8)$$

where, U_j^0 and i_j^0 are respectively the standard potential and exchange current density of an electrochemical reaction j , whereas E is the working electrode potential.

The total electrode current (I_t) is calculated with Equation (9),

$$I_t = A \sum_j i_j \quad (9)$$

where A [Eq. (10)] is the active surface area of the working electrode, which is the product of the volume of the bin closest to the electrode ($V_{x=0}^{bin}$) and the active specific surface area [a is calculated using Eq. (13)],

$$A = a V_{x=0}^{bin} \quad (10)$$

Finally, G_i is the source/sink term related to the heterogeneous dissolution/precipitation of sulfur based solid species over the electrode [Eq. (11)].^[34]

$$G_i = \sum_k \gamma_{ik} k_k^{prec} \varepsilon_k \left(\prod_i (c_i)^{\gamma_{ik}} - K_k^{sp} \right) \quad (11)$$

It should be noted that the G_i is zero in all the bins except in the closest one to the electrode surface. In the equation above, γ_{ik} is the stoichiometric coefficient of the species i involved in the dissolution/precipitation reaction of the sulfur based solid species k (see Supporting Information). K_k^{sp} and ε_k are respectively the solubility product and the volume fraction of a sulfur based solid species. k_k^{prec} is the rate constant of precipitation/dissolution reaction of k and ε_k is given by the solution of

$$\frac{d\varepsilon_k}{dt} = V_k \varepsilon_k k_k^{prec} \left(\prod_i (c_i)^{\gamma_{ik}} - K_k^{sp} \right) \quad (12)$$

In the equation above, V_k is the molar volume of the sulfur based solid species. Since sulfur based solid species such as $S_{8(s)}$ and $Li_2S_{(s)}$ are insulating, their precipitation over the surface of the working electrode reduces the active surface (a) due to surface passivation [Eq. (13)]:

$$a = a^0 \Theta(\delta) \quad (13)$$

where a^0 and $\Theta(\delta)$ are the initial specific surface area of the working electrode ($a^0 = A^0 / V_{x=0}^{bin}$) and the electron tunneling probability function^[35] given by

$$\Theta(\delta) = \frac{1 - erf\left(\frac{\delta - \delta_{tun}}{L_{tun}}\right)}{2} \quad (14)$$

In Equation (14), δ_{tun} and L_{tun} are the threshold thickness at halved electron tunneling and the scaling factor, respectively. δ is the total thickness of sulfur-based solid deposits on the working electrode,

$$\delta = \frac{\sum_k \varepsilon_k}{a^{max}} \quad (15)$$

2.2. Computational Implementation

The model was implemented in the MATLAB software and the coupled partial differential equations were solved spatially using the Finite Volume Method and temporally using the Crank-Nicholson (see Supporting Information) and Newton-Ralphson methods. The CV characteristics are very sensitive to the kinetic and the diffusion parameters values. Therefore, we have used the parameter values which are available in the literature as much as possible (Tables 1–4). However well-defined experimental values are not available for certain parameters such as the exchange current densities or the charge transfer coefficients of different polysulfides reactions in 1 M LiTFSI in TEGDME:DOL. Therefore, the initial values of those parameters were determined using an automatized MATLAB program, which matches the reduction part of the simulated CVs of different polysulfides containing solutions with their corresponding experimental results using a nonlinear least-squares solver called lsqnonlin. The initial values of the

Table 1. Electrochemical reaction parameters.

Reaction No. (j)	Reactions	i_j^0 [A] ^[a]	U_j^0 [V] ^[a]	α
1	S_8 / S_8^{2-}	0.150	-0.8281	0.46 ^[b]
2	S_8^{2-} / S_6^{2-}	3×10^{-3}	-0.8681	0.50 ^[d]
3	S_6^{2-} / S_4^{2-}	4×10^{-4}	-0.9400	0.420 ^[c]
4	S_4^{*-} / S_4^{2-}	2×10^{-3}	-0.9400	0.50 ^[d]
5	S_4^{2-} / S_2^{2-}	2.96×10^{-6}	-1.0544	0.20 ^[a]
6	S_3^{*-} / S_3^{2-}	7.4×10^{-2}	-1.1644	0.42 ^[a]
7	S_3^{2-} / S_2^{2-}	1.48×10^{-7}	-1.2044	0.35 ^[a]
8	S_2^{2-} / S^{2-}	1×10^{-9}	-1.2200	0.50 ^[d]

[a] Fitted parameters. [b], [c] and [d] are parameters taken from Ref. [15], Ref. [35] and Ref. [22], respectively.

Table 2. Chemical reaction parameters.

Reaction No. (j)	Reactions	k_j^f [s ⁻¹] ^[a]	K_j^{eq} [mol ⁻¹] ^[a]
1	$S_8^{2-} \rightleftharpoons 2S_4^{*-}$	8.4	4.2088
2	$S_6^{2-} \rightleftharpoons 2S_3^{*-}$	9.5	12.6263

[a] Fitted parameters.

Table 3. Precipitation/dissolution reaction parameters.

Reaction No. (<i>j</i>)	Reactions	k_k^{prec} [mol ² .m ⁻⁶ s ⁻¹]	K_k^{sp} [mol ³ .m ⁻⁹]
1	$S_8 \rightleftharpoons S_{8(s)}$	$5\text{ (s}^{-1}\text{)}^{[a]}$	$6\text{ [mol.m}^{-3}\text{]}^{[b]}$
2	$2Li^+ + S^{2-} \rightleftharpoons Li_2S_{(s)}$	$5 \times 10^{-7}[c]$	$10^{[c]}$

[a], [b] Fitted and measured parameters, respectively. [c] Parameters taken from Ref. [35].

Table 4. Diffusion coefficients of dissolved species in the electrolyte.

Species No. (<i>j</i>)	Species symbol	D_i [m ² .s ⁻¹]
1	Li^+	$0.7 \times 10^{-10}[b]$
2	S_8	$1.7 \times 10^{-10}[a]$
3	S_8^{2-}	$8.0 \times 10^{-11}[a]$
4	S_6^{2-}	$8.0 \times 10^{-11}[c]$
5	S_4^{*-}	$3.5 \times 10^{-11}[d]$
6	S_4^{2-}	$3.5 \times 10^{-11}[d]$
7	S_3^{*-}	$3.5 \times 10^{-11}[d]$
8	S_3^{2-}	$3.5 \times 10^{-11}[d]$
9	S_2^{2-}	$3.5 \times 10^{-11}[d]$
10	S^{2-}	$3.5 \times 10^{-11}[d]$

[a] Fitted parameters. [b] Calculated parameters taken from Ref. [36]. [c] Parameter taken from Ref. [35]. [d] Experimentally determined parameters from Ref. [37].

unknown parameters are determined piece wise, where a set of one or two parameters are fitted during a run of this automatized MATLAB program and then the process is repeated for another set. These initial values of parameters were further adjusted until we were able to match all the simulated results as close as possible with the experimental ones. The parameters chosen for the cyclic voltammetry model are given in Tables 1–4. It should be noted that a single set of parameter values was found and used to simulate all the experimental CVs recorded under different operation conditions.

The concentration of the species at the electrode surface are determined implicitly by solving a set of non-linear equations using the Newton-Raphson method. If the initial concentrations of the dissolved species are zero, the solutions of these non-linear equations will be infinities. Therefore, in our model we assume trace values for the concentrations of polysulfides which should not be present in the experimental electrolyte solution (see Table S1 in Supporting Information).

3. Results and Discussion

The experimental CV of 6 mM S_8 in 1 M LiTFSI in TEGDME:DOL recorded at 5 mV.s⁻¹, consists of two reduction (R_1 and R_2) and two oxidation (OXI₁ and OXI₂) peaks (Figure 3). Initially, the simulation of the CV of 6 mM S_8 solution at 5 mV.s⁻¹ (Figure 3) was done using the following set of reaction steps [Eqs. (16)–

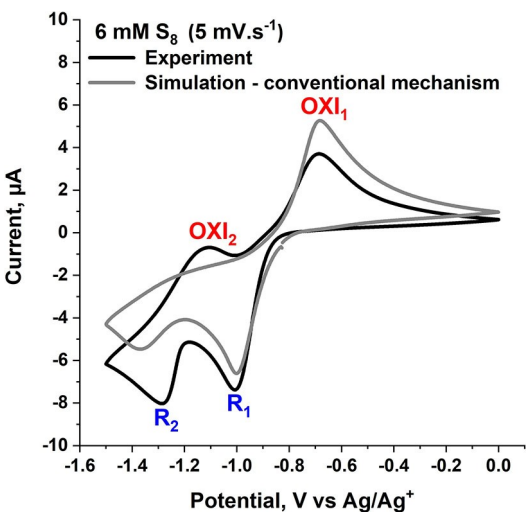


Figure 3. Experimental CV of 6 mM S_8 in 1 M LiTFSI in TEGDME:DOL measured at 5 mV.s⁻¹ and the corresponding simulated CV produced using the conventional reaction mechanism of Li–S batteries models [Eqs. (16) to (22)].

(22)] which is conventionally used in continuum Li–S batteries models,^[34,38–41]



The initial simulated CV of S_8 (Figure 3), produced using the conventional reaction mechanism consists of two reduction peaks R_1 and R_2 and one oxidation peak OXI₁. However, the oxidation peak OXI₂ is absent in the simulated CV (Figure 3). This indicates that the polysulfide intermediates which undergo oxidation around OXI₂ are not considered in the conventionally used reaction mechanism [Eqs. (16) to (22)]. Furthermore, the experimental peak intensity of OXI₂ does not increase with the scan rate as much as the intensities of other peaks namely R_1 , R_2 and OXI₁ (Figure 4). This suggests that the underlying reaction mechanism behind OXI₂ should implicate some electrochemical reactions which are coupled to other chemical reactions. Therefore, these aforementioned characteristics trends of OXI₂ cannot be reproduced by our CV model using

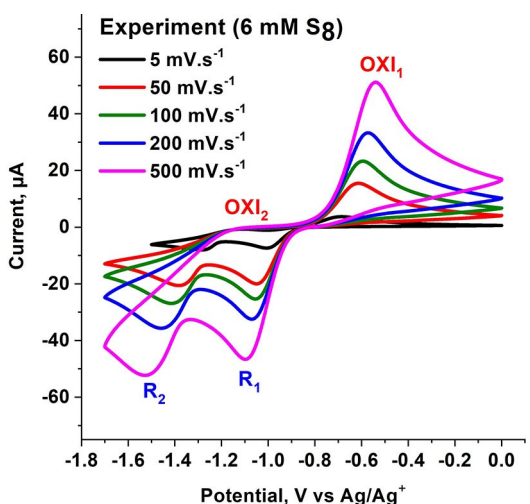


Figure 4. Experimental CVs of 6 mM S₈ in 1 M LiTFSI in TEGDME:DOL recorded with different scan rates.

only the reaction steps [Eqs. (16) to (22)] considered in the conventional reaction mechanism. We also arrived at this conclusion after an extensive parameter analysis. Furthermore, our model cannot simulate the variation of the second oxidation peak (OXI₂) intensity with the scan rate and initial polysulfide speciation without the inclusion of the reaction steps involving S₃^{*-} and S₃²⁻ [Eqs. (25) to (27)]. These issues cannot be fixed by using simpler reaction mechanisms and adjusting the corresponding parameters. This aforementioned claim was demonstrated in the Supporting Information using the simulated CVs produced using a simpler reaction mechanism which do not include reactions involving S₃^{*-} and S₃²⁻.

Various studies in the literature involving the spectroscopic analysis of dissolved polysulfides in the electrolyte, have shown that the presence of the polysulfide ions and radicals primarily depend on the properties of the solvents such as the donor numbers and dielectric constants.^[4,42] More specifically, *in situ* and operando Raman spectroscopic studies have proven that the polysulfide radicals such as S₄^{*-} and S₃^{*-} are produced during the operation of Li-S cells containing LiTFSI in TEGDME:DOL.^[43,44] Furthermore Karaseva *et al.*, suggested that electrolytes such as sulfolane containing 1 M lithium salt are optimum for producing polysulfide radicals due to the availability of free and unbound solvent molecules in them which assists in the proper utilization of polysulfide species.^[45] Therefore, the reaction mechanism described through Eqs. (16)–(22) in the cyclic voltammetry model was replaced with a comprehensive set of reaction steps [Eqs. (16) to (27)] which includes the following chemical and electrochemical reactions of S₄^{*-} and S₃^{*-},



Eqs. (23) to (26) have been proposed in a previously reported cyclic voltammetry model which was used to simulate the CVs of dissolved Li₂S₆ in DMF,^[22] while the S₃²⁻/S₂²⁻ redox reaction was proposed in the experimental work by Barschaz *et al.*^[6]

The simulated CV of 6 mM S₈ solution at 5 mV.s⁻¹ produced using the comprehensive reaction mechanism described through the Eqs. (16) to (27), closely resembles the experimental one, where the OXI₂ peak has been reproduced (Figure 5). The underlying reaction steps behind the cyclic voltammetry peaks could be assessed from the evolutions of simulated individual redox reaction currents and polysulfides concentrations at the electrode surface.

During the oxidation scan of 6 mM S₈ solution at 5 mV.s⁻¹, the S₃^{*-}/S₃²⁻ reaction current produces an intense positive peak around -1.3 V (Figure 6), which is the reason behind the visibility of OXI₂ (Figure 5). The concentration of S₃^{*-} increases between -1.5 to -1.1 V due to the oxidation of S₃²⁻ (see Figure S5a in Supporting Information).

Since the S₃^{*-}/S₃²⁻ reaction current is kinetically controlled by the dissociation of S₆²⁻, its peak intensities do not increase significantly when the potential scan rate is increased (Figure 7a), therefore the peak OXI₂ becomes visibly indistinctive during fast scan rates (Figures 4 and 7b).

It has been hypothesized that due to the low electron densities over the chains of the polysulfide radicals their electrochemical reaction kinetics are faster than those of the polysulfide ions.^[45] The fitted exchange current density of S₃^{*-}/S₃²⁻ reaction in our model is in agreement with this hypothesis,

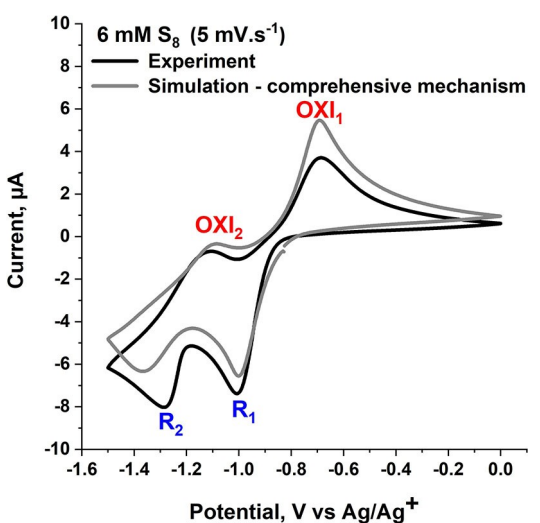


Figure 5. Experimental CV of 6 mM S₈ in 1 M LiTFSI in TEGDME:DOL measured at 5 mV.s⁻¹ and the corresponding simulated CV produced using the reaction mechanism described through [Eqs. (16) to (27)].

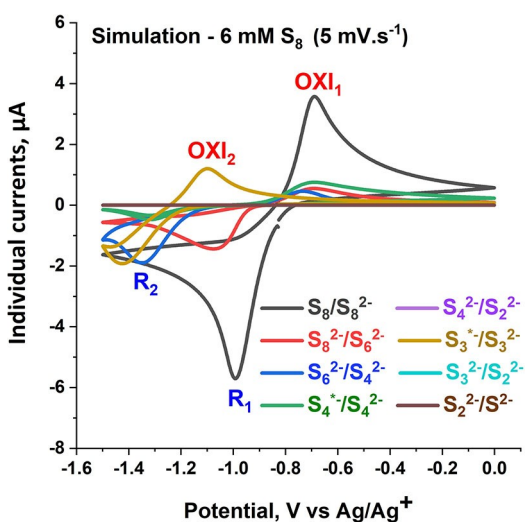


Figure 6. Simulated individual redox reaction currents corresponding to the CV of 6 mM S_8 solution at $5\text{ mV}\cdot\text{s}^{-1}$, produced using the comprehensive reaction mechanism [Eqs. (16) to (27)].

since its value is larger than those of the reactions involving only the polysulfide ions (Table 1).

During the reduction scan of 6 mM S_8 solution at $5\text{ mV}\cdot\text{s}^{-1}$, S_8/S_8^{2-} and S_8^{2-}/S_6^{2-} electrochemical reaction currents produce peaks around -1.0 V and -1.1 V (Figure 6), respectively. Therefore, these are the underlying dominant reactions behind the reduction peak R_1 (Figure 5). This can also be understood from the evolutions of both S_8 and S_8^{2-} concentrations (Figure 8), since they decrease significantly below -1.0 V during the reduction scan.

The characteristics of the first CV of 50 mM Li_2S_8 solution are different from those of S_8 , since the intensity of its reduction peak R_1 is significantly lower than that of its R_2 (Figure 9a). Whereas, R_1 is completely invisible in the first CV of 50 mM Li_2S_6 solution (Figure 10a). These results indicate that

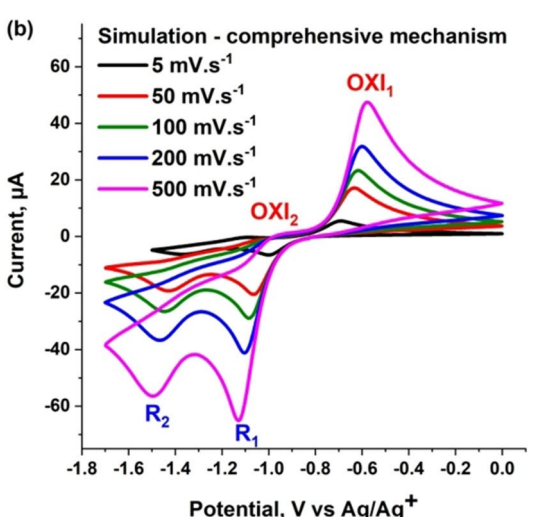
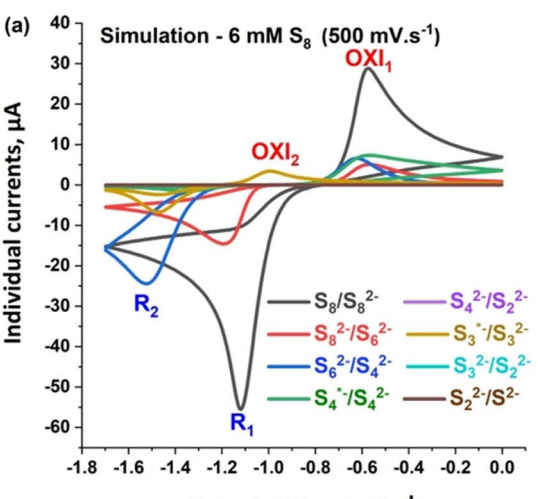


Figure 7. a) Simulated individual redox reaction currents corresponding to the CV of 6 mM S_8 solution at $500\text{ mV}\cdot\text{s}^{-1}$ and b) the simulated CVs of S_8 at different scan rates, produced using the comprehensive reaction mechanism [Eqs. (16) to (27)].

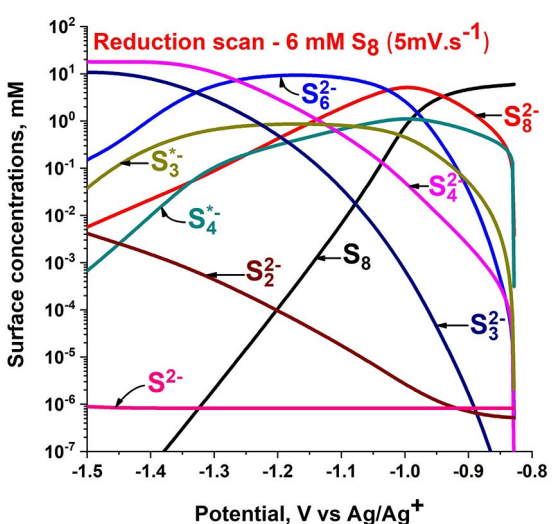


Figure 8. Simulated species concentrations at the electrode surface ($(c_i)_{x=0}$) during the reduction scan of 6 mM S_8 solution at $5\text{ mV}\cdot\text{s}^{-1}$.

the characteristics of the initial CV primarily depend on the type of the polysulfide species initially present in the electrolyte. In general, the intensities of all the distinctive peaks (R_1 , R_2 and OXI_1) in the CVs of Li_2S_8 and Li_2S_6 solutions are higher (Figures 9a and 10a) than those of S_8 (Figure 4 and 7b). This is due to the increase of the polysulfides concentrations in the 50 mM Li_2S_8 and Li_2S_6 solutions.

In order to simulate the CVs of Li_2S_8 and Li_2S_6 solutions, the initial concentrations of S_8^{2-} and S_6^{2-} were set to 50 mM. As mentioned in the computational implementation subsection, trace amounts are assumed for the concentrations of all the other polysulfides (Table S1). The characteristics of the simulated CVs (Figures 9b and 10b) qualitatively resemble the experimental ones (Figure 9a and 10a).

Since S_8 is initially absent in the 50 mM Li_2S_8 solution, the S_8/S_8^{2-} reaction current does not produce an intense peak during the first reduction scan (Figure 11a). While, only the

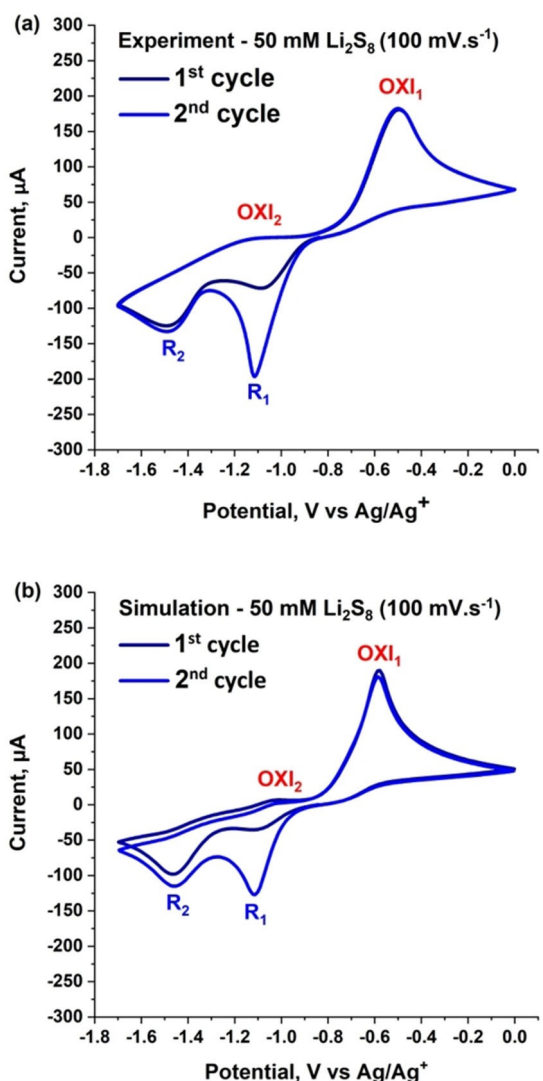


Figure 9. a) Experimental and b) simulated CVs of 50 mM Li₂S₈ solution produced using the potential scan rate of 100 mV.s⁻¹.

S_8^{2-}/S_6^{2-} reaction current produces an intense peak around -1.10 V (Figure 11a). The absence of intense S_8/S_8^{2-} reaction current peak around -1.10 V (Figure 11a) is the reason why the intensity of R₁ is relatively lower during the first reduction scan (Figures 9a and b).

Similarly S_8 and S_8^{2-} are initially absent in the 50 mM Li₂S₆ solution. Therefore, the individual currents of S_8/S_8^{2-} and S_8^{2-}/S_6^{2-} reactions do not form intense peaks during the first reduction scan (Figure 11b). Therefore, the reduction peak R₁ does not appear during this scan (Figures 10a and b).

The individual currents of S_6^{2-}/S_4^{2-} , S_4^{*-}/S_4^{2-} and S_3^{*-}/S_3^{2-} produce peaks between -1.3 to -1.5 V during the reduction scans of the 6 mM S₈ solution at different rates (Figures 6 and 7a). Whereas, these peaks are produced around -1.5 V during the first reduction scan of 50 mM Li₂S₈ solution at 100 mV.s⁻¹ (Figure 11a).

The CV characteristics of Li₂S₆ in 1 M LiTFSI in TEGDME:DOL are different from those of Li₂S₆ in DMF and NH₃ reported in

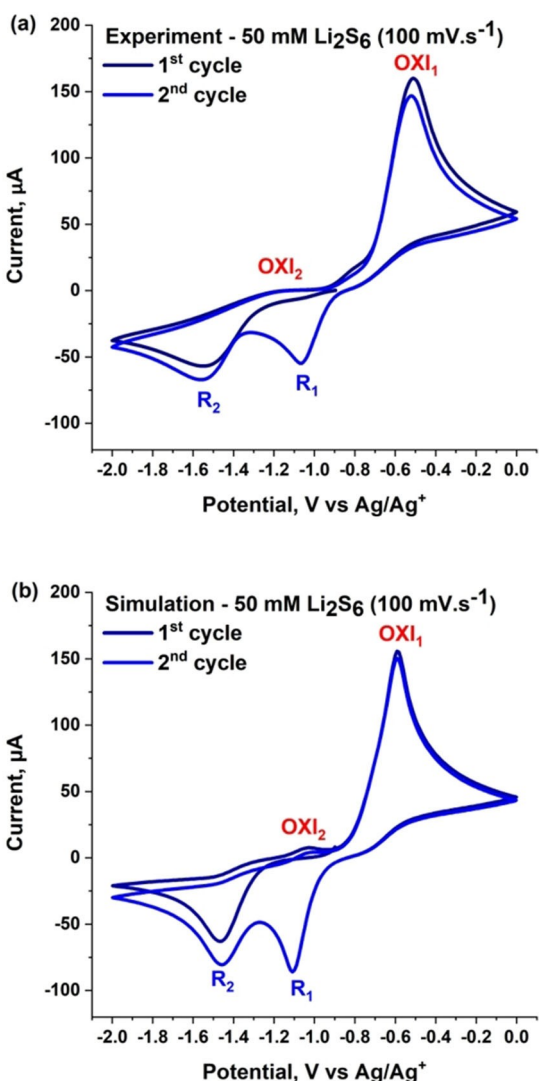


Figure 10. a) Experimental and b) simulated CVs of 50 mM Li₂S₆ solution produced using the potential scan rate of 100 mV.s⁻¹.

the works by Gaillard *et al.*^[22] and Levillain *et al.*^[23] respectively. The CVs of Li₂S₆ in DMF consists of two reduction peaks namely R₄ and R₃ which correspond to reductions of S_4^{*-} and S_3^{*-} , respectively. While the CVs of Li₂S₆ in NH₃ also consists of two reduction peaks namely R₁ and R₂ which correspond to one electron reductions of S_3^{*-} and S_6^{2-} that produce S_3^{2-} and S_6^{3-} , respectively. Whereas, the 1st CV of Li₂S₆ in 1 M LiTFSI in TEGDME:DOL consists of only one reduction peak (R₂) (Figure 10) and our simulated results show that the reductions of S_6^{2-} and S_3^{*-} occur simultaneously during the R₂ peak (Figure 11b). Additionally, the simulated results of the 1st reduction scan of Li₂S₈ in 1 M LiTFSI show that the reduction S_4^{*-} also take place during R₂ (Figure 11a). Since S_4^{*-} radical is produced by the dissociation of S_8^{2-} , the invisibility of the S_4^{*-}/S_4^{2-} reaction current during the first reduction of scan of Li₂S₆ solution (Figure 11b) is due to the initial absence of S_8^{2-} in it. Therefore, S_6^{2-}/S_4^{2-} , S_4^{*-}/S_4^{2-} and S_3^{*-}/S_3^{2-} reactions occur

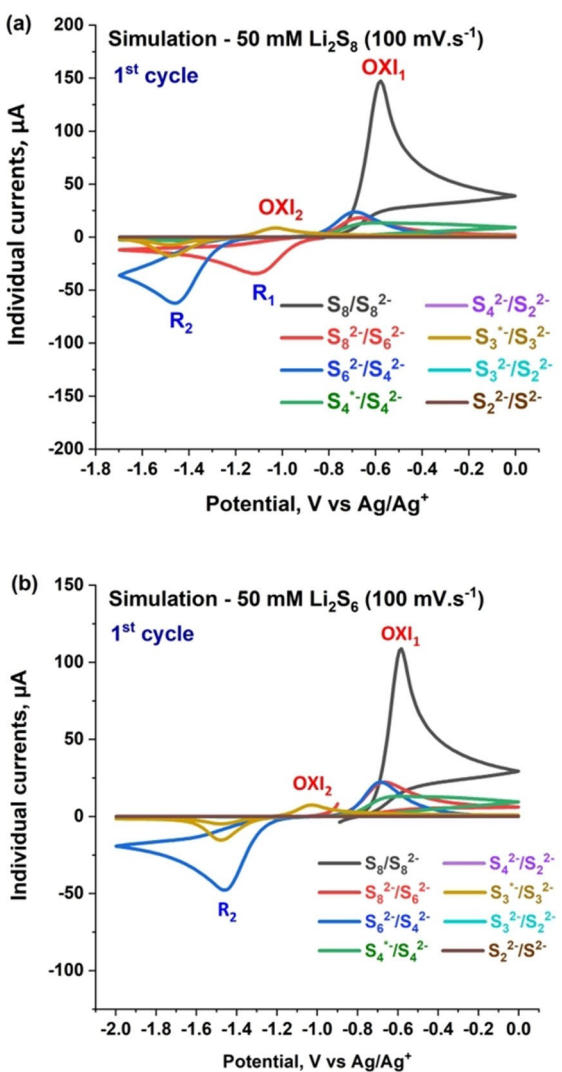


Figure 11. Simulated individual currents of electrochemical reactions during the first CV cycles of a) 50 mM Li_2S_8 and b) 50 mM Li_2S_6 solutions, with a scan rate of 100 mV.s⁻¹.

simultaneously during the reduction peak R_2 (Figures 6, 7a, 11 and 12), which is a new insight provided by our model.

The dominant reactions behind R_2 could also be understood from the decrease of S_6^{2-} , S_3^{*-} and S_4^{*-} concentrations around -1.3 V during the reduction of scan of 6 mM S_8 solution at 5 mV.s⁻¹ (Figure 8). Whereas, the concentrations of S_4^{2-} and S_3^{2-} continue increase around -1.3 V. The negligible increase of S_2^{2-} concentration is due to the reduction reactions of S_4^{2-} and S_3^{2-} . However, the S_4^{2-} and S_3^{2-} concentrations do not decrease significantly at the end of reduction scan due to the sluggish kinetics of their reduction reactions.

During oxidation scans and the periods leading up to the oxidation peak OXI_2 (Figures 6 and 11a), the concentrations of S_2^{2-} and S_4^{2-} decrease due to their oxidations to S_3^{2-} and S_6^{2-} , respectively (Figures S5a and b in the Supporting Information). Furthermore, S_3^{2-} concentration start to decrease significantly (Figures S5a and b) around OXI_2 (Figures 6 and 11a). However, the oxidation peak OXI_2 is not visible in the CVs of Li_2S_8 and

Li_2S_6 solutions (Figures 9 and 10), due to their fast scan rate of 100 mV.s⁻¹. Around -0.6 V, concentrations of all the polysulfides ions and radicals decrease significantly, while the S_8 concentration increases (Figures S5a and b in the Supporting Information). This indicates that all the polysulfides simultaneously undergo oxidation to produce S_8 . This is also evident from the individual current peaks of $\text{S}_4^{*-}/\text{S}_4^{2-}$, $\text{S}_6^{2-}/\text{S}_4^{2-}$, $\text{S}_8^{2-}/\text{S}_4^{2-}$, S_6^{2-} and S_8^{2-} redox reactions around -0.6 V (Figures 6, 7a and 11), which form the basis for the oxidation peak OXI_1 (Figures 4, 9 and 10).

Since S_8 becomes a dominant species near the electrode surface in the Li_2S_8 (Figure S5b in the Supporting information) and Li_2S_6 solutions at the end of the first oxidation scan, the S_8^{2-} and $\text{S}_8^{2-}/\text{S}_6^{2-}$ reaction currents form intense peaks around -1.1 V during the second reduction scans (Figures 12a and b). Therefore, the peak intensity of R_1 increases during the second reduction scan of the Li_2S_8 solution (Figures 9a and b). Whereas, the reduction peak R_1 becomes visible during the second reduction scan of the Li_2S_6 solution (Figures 10a and b).

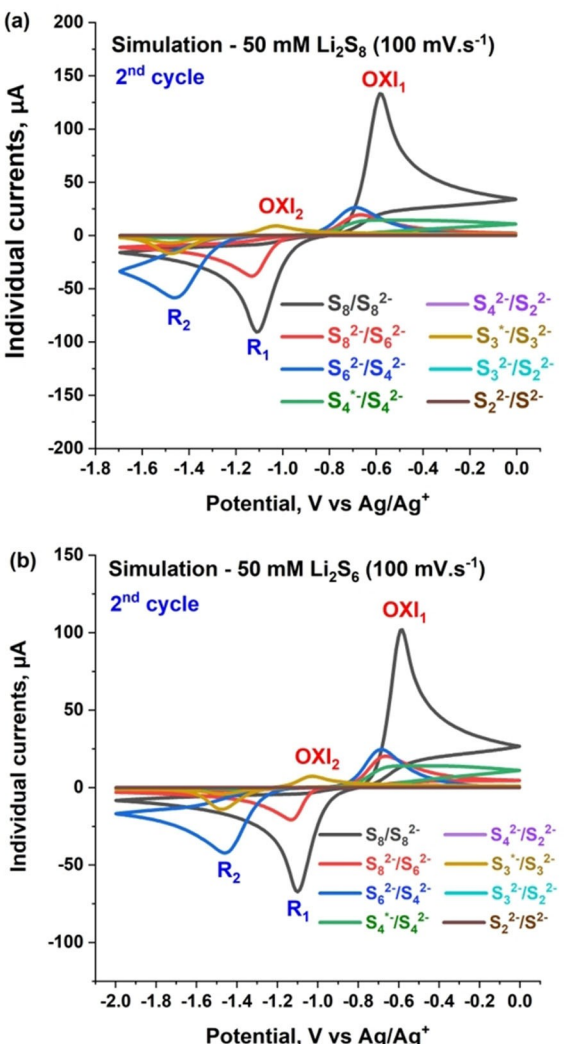


Figure 12. Simulated individual currents of electrochemical reactions during the second CV cycles of a) 50 mM Li_2S_8 and b) 50 mM Li_2S_6 solutions, with a scan rate of 100 mV.s⁻¹.

The rest of the characteristics of the second CVs of 50 mM Li_2S_8 and Li_2S_6 solutions are similar to those of the corresponding first curves. Throughout the reduction and oxidation scans of all the cyclic voltammetry simulations, the Li^+ concentration and volume fractions of $\text{S}_{8(\text{s})}$ and $\text{Li}_2\text{S}_{(\text{s})}$ at the electrode surface do not change in any significant way (see Figure S6 in the Supporting Information). This suggests that the depositions of $\text{S}_{8(\text{s})}$ and $\text{Li}_2\text{S}_{(\text{s})}$ over the working electrode surface are negligible.

In summary, $\text{S}_8/\text{S}_8^{2-}$ and $\text{S}_8^{2-}/\text{S}_6^{2-}$ electrochemical reactions form the underlying basis of the reduction peak R_1 , while $\text{S}_6^{2-}/\text{S}_4^{2-}$, $\text{S}_4^{*-}/\text{S}_4^{2-}$ and $\text{S}_3^{2-}/\text{S}_3^{*-}$ reactions occur simultaneously during R_2 . The oxidation of S_3^{2-} to S_3^{*-} dominate the oxidation peak OXL_2 , whereas all the polysulfides ions and radicals get oxidized to S_8 around OXL_1 .

4. Conclusions

CV investigations of different polysulfides solutions, using our relatively simple experimental setup, have shown that the complex CV characteristics depend primarily on the type and concentration of the initially dissolved polysulfide in the electrolyte. The initial polysulfides speciation in the electrolyte influences the CV characteristics, even if the Pt counter electrode is replaced with Li, which has been previously observed experimentally by Zheng *et al.*^[46] The characteristics also depend on the scan rate and cycle number. The combination of this type of experiments with modelling can assist in determining the reaction steps that explain the reasons behind the changes in the CV characteristics under a wide range of experimental conditions (e.g. initial dissolved polysulfide speciation and scan rate). There are various analytical spectroscopic tools such as the UV-vis, Raman, etc. which already assist in the measurement of the evolutions of different polysulfides in the electrolyte during the operation of Li–S batteries.^[3,6–8] However, the studies using these tools hypothesize reaction mechanisms with a large number of reaction steps. Therefore, modelling the CVs of dissolved sulfur and polysulfides can assist in verifying the plausibility of the hypothesized reaction steps.

The initial simulated CV of S_8 produced using the conventionally assumed reaction mechanism of Li–S batteries models, could not reproduce the oxidation peak OXL_2 and its characteristic changes with the scan rate. This shows that the reaction steps of the conventionally assumed reaction mechanism are insufficient for simulating the entire CV characteristics of dissolved S_8 in 1 M LiTFSI in TEGDME:DOL and their variation with operation conditions. The CV simulation results produced using our comprehensive reaction mechanism, have revealed that the visibility of the oxidation peak OXL_2 depends on the intensity of the $\text{S}_3^{*-}/\text{S}_3^{2-}$ reaction current peak. This result confirms the presence of S_3^{*-} radical and its redox reaction in 1 M LiTFSI in TEGDME:DOL. Furthermore, the fitted exchange current density of $\text{S}_3^{*-}/\text{S}_3^{2-}$ reaction shows that its electrochemical reaction kinetics is faster than those involving only the polysulfide ions. It also indicates that the modelling of the

CV curves not only helps in identifying the initial speciation of dissolved polysulfide in the electrolyte, but it also assists in identifying the presence of some polysulfide intermediates as well. Ideally, all the possible elementary reaction steps involving polysulfides in 1 M LiTFSI in TEGDME:DOL should be included to the conventional reaction mechanism [Eqs. (16) to (22)]. However, including a very large number of reaction steps would further complicate our model due to the increase of unknown parameters. Since our simulated CVs have good semi-quantitative agreement with a wide range of experiments, the reaction steps considered [Eqs. (16) to (27)] in our model are sufficiently comprehensive. However, our comprehensive reaction mechanism could be further expanded if it is necessary to explain some newer experimental observations of cyclic voltammetry of polysulfides in 1 M LiTFSI in TEGDME:DOL using our model. Furthermore, the mathematical description of our model along with an appropriate reaction mechanism could be used to simulate the CVs of dissolved sulfur and polysulfides in any Li–S battery electrolyte.

Our simulation results show that unlike the CVs of Li_2S_6 in DMF^[22] and NH_3 ,^[23] the R_2 peak of Li_2S_6 in 1 M LiTFSI in TEGDME:DOL corresponds to the simultaneous reductions of S_6^{2-} , S_4^{*-} and S_3^{*-} . Simulation results have also shown that the increase in the intensity and appearance of CV peaks during the second cycle as in the case of Li_2S_8 and Li_2S_6 solutions respectively, are due to the occurrence of additional electrochemical reactions and change in the polysulfide speciation at the end of the first cycle. This effect should be considered during the characterization of dissolved polysulfides using continuous cycling as in the study of effectiveness of polysulfide crossover blocking by an ion-selective membrane.^[18,47]

Acknowledgements

We deeply acknowledge Dr. Charles Delacourt (LRCS) for very useful discussions at the beginning of this work. Discussions with Prof. Patrik Johansson (Chalmers University of Technology) are also highly appreciated. The authors are deeply thankful to the European Union's Horizon 2020 research and innovation programme for funding support through the HELIS project under grant agreement No. 314515. AAF deeply acknowledges the Institut Universitaire de France for the support.

Conflict of Interest

The authors declare no conflict of interest.

Keywords: polysulfides · reaction steps · polysulfides intermediates · cyclic voltammetry · mathematical model · lithium-sulfur batteries

- [1] S. Walus, Lithium/Sulfur Batteries: Development and Understanding of the Working Mechanisms, Université Grenoble Alpes, 2015.
- [2] L. F. Nazar, M. Cuisinier, Q. Pang, *MRS Bull.* 2014, 39, 436–442.

- [3] Q. Zou, Y.-C. Lu, *J. Phys. Chem. Lett.* **2016**, *7*, 1518–1525.
- [4] K. H. Wujcik, D. R. Wang, A. Raghunathan, M. Drake, T. A. Pascal, D. Prendergast, N. P. Balsara, *J. Phys. Chem. C* **2016**, *120*, 18403–18410.
- [5] Q. He, Y. Gorlin, M. U. M. Patel, H. A. Gasteiger, Y.-C. Lu, *J. Electrochem. Soc.* **2018**, *165*, A4027–A4033.
- [6] C. Barchasz, F. Molton, C. Duboc, J.-C. Leprêtre, S. Patoux, F. Alloin, *Anal. Chem.* **2012**, *84*, 3973–3980.
- [7] Y. Gorlin, M. U. M. Patel, A. Freiberg, Q. He, M. Piana, M. Tromp, H. A. Gasteiger, *J. Electrochem. Soc.* **2016**, *163*, A930–A939.
- [8] J. Conder, R. Bouchet, S. Trabesinger, C. Marino, L. Gubler, C. Villevieille, *Nat. Energy* **2017**, *2*, 17069–17075.
- [9] M. V. Merritt, D. T. Sawyer, *Inorg. Chem.* **1970**, *9*, 211–215.
- [10] N. Xie, Y. Huang, *Acta Chim. Sin.* **1989**, *47*, 227–232.
- [11] N. Xie, Y. Huang, *Acta Chim. Sin.* **1988**, *46*, 631–638.
- [12] B.-S. Kim, S.-M. Park, *J. Electrochem. Soc.* **1993**, *140*, 115–122.
- [13] D.-H. Han, B.-S. Kim, S.-J. Choi, Y. Jung, J. Kwak, S.-M. Park, *J. Electrochem. Soc.* **2004**, *151*, E283–E290.
- [14] F. Gaillard, E. Levillain, *J. Electroanal. Chem.* **1995**, *398*, 77–87.
- [15] Y. Jung, S. Kim, B.-S. Kim, D.-H. Han, S.-M. Park, J. Kwak, *Int. J. Electrochem. Sci.* **2008**, *3*, 566–577.
- [16] N. S. A. Manan, L. Aldous, Y. Alias, P. Murray, L. J. Yellowlees, M. C. Lagunas, C. Hardacre, *J. Phys. Chem. B* **2011**, *115*, 13873–13879.
- [17] H. Yamin, A. Gorenstein, J. Penciner, Y. Sternberg, E. Peled, *J. Electrochem. Soc.* **1988**, *135*, 1045–1048.
- [18] C. Li, A. L. Ward, S. E. Doris, T. A. Pascal, D. Prendergast, B. A. Helms, *Nano Lett.* **2015**, *15*, 5724–5729.
- [19] S. E. Doris, A. L. Ward, P. D. Frischmann, L. Li, B. A. Helms, *J. Mater. Chem. A* **2016**, *4*, 16946–16952.
- [20] X. Huang, Z. Wang, R. Knibbe, B. Luo, S. A. Ahad, D. Sun, L. Wang, *Energy Technol.* **2019**, *7*, 1801001.
- [21] E. Levillain, F. Gaillard, P. Leghie, A. Demortier, J. P. Lelieur, *J. Electroanal. Chem.* **1997**, *420*, 167–177.
- [22] F. Gaillard, E. Levillain, J. P. Lelieur, *J. Electroanal. Chem.* **1997**, *432*, 129–138.
- [23] E. Levillain, A. Demortier, J. P. Lelieur, *J. Electroanal. Chem.* **1995**, *394*, 205–210.
- [24] M. Mačák, P. Vyroubal, T. Kazda, K. Jaššo, *J. Energy Storage* **2020**, *27*, 101158.
- [25] S. Hess, M. Wohlfahrt-Mehrens, M. Wachtler, *J. Electrochem. Soc.* **2015**, *162*, A3084–A3097.
- [26] M. R. Kaiser, S. Chou, H.-K. Liu, S.-X. Dou, C. Wang, J. Wang, *Adv. Mater.* **2017**, *29*, 1700449.
- [27] D. Di Lecce, L. Carbone, V. Gancitano, J. Hassoun, *J. Power Sources* **2016**, *334*, 146–153.
- [28] V. Thangavel, M. Morcrette, A. Franco, “HELIIS project D6.2 deliverable report - databases for results produced using interfacial models,” can be found under https://www.helis-project.eu//docstation/com_content/article/181/helis_project_deliverable_d6_2_final.pdf, 2017.
- [29] Y.-C. Lu, Q. He, H. A. Gasteiger, *J. Phys. Chem. C* **2014**, *118*, 5733–5741.
- [30] D. Zheng, X. Zhang, J. Wang, D. Qu, X. Yang, D. Qu, *J. Power Sources* **2016**, *301*, 312–316.
- [31] A. Evans, M. I. Montenegro, D. Pletcher, *Electrochim. Commun.* **2001**, *3*, 514–518.
- [32] J. W. Dibden, N. Meddings, J. R. Owen, N. Garcia-Araez, *ChemElectroChem* **2018**, *5*, 445–454.
- [33] R. G. Compton, E. Laborda, K. R. Ward, *Understanding Voltammetry: Simulation of Electrode Processes*, Imperial College Press, London, **2014**.
- [34] K. Kumaresan, Y. Mikhaylik, R. E. White, *J. Electrochem. Soc.* **2008**, *155*, A576–A582.
- [35] V. Thangavel, K.-H. Xue, Y. Mammeri, M. Quiroga, A. Mastouri, C. Guéry, P. Johansson, M. Morcrette, A. A. Franco, *J. Electrochim. Soc.* **2016**, *163*, A2817–A2829.
- [36] S. Osella, A. Minoia, C. Quartì, J. Cornil, R. Lazzaroni, A. Goffin, M. Guillaume, D. Beljonne, *Batteries Supercaps* **2019**, *2*, 473–481.
- [37] S. Drvarić Talian, J. Moškon, R. Dominko, M. Gaberšček, *ACS Appl. Mater. Interfaces* **2017**, *9*, 29760–29770.
- [38] M. Ghaznavi, P. Chen, *Electrochim. Acta* **2014**, *137*, 575–585.
- [39] M. Ghaznavi, P. Chen, *J. Power Sources* **2014**, *257*, 394–401.
- [40] T. Zhang, M. Marinescu, S. Walus, P. Kovacik, G. J. Offer, *J. Electrochim. Soc.* **2018**, *165*, A6001–A6004.
- [41] T. Zhang, M. Marinescu, S. Walus, G. J. Offer, *Electrochim. Acta* **2016**, *219*, 502–508.
- [42] M. Cuisinier, C. Hart, M. Balasubramanian, A. Garsuch, L. F. Nazar, *Adv. Energy Mater.* **2015**, *5*, 1401801.
- [43] H.-L. Wu, L. A. Huff, A. A. Gewirth, *ACS Appl. Mater. Interfaces* **2015**, *7*, 1709–1719.
- [44] J. Hannauer, J. Scheers, J. Fullenwarth, B. Fraisse, L. Stievano, P. Johansson, *ChemPhysChem* **2015**, *16*, 2755–2759.
- [45] E. V. Karaseva, E. V. Kuzmina, D. V. Kolosnitsyn, N. V. Shakirova, L. V. Sheina, V. S. Kolosnitsyn, *Electrochim. Acta* **2019**, *296*, 1102–1114.
- [46] D. Zheng, X. Zhang, J. Wang, D. Qu, X. Yang, D. Qu, *J. Power Sources* **2016**, *301*, 312–316.
- [47] S. E. Doris, A. L. Ward, P. D. Frischmann, L. Li, B. A. Helms, *J. Mater. Chem. A* **2016**, *4*, 16946–16952.

Manuscript received: July 21, 2020

Revised manuscript received: August 29, 2020

Accepted manuscript online: August 31, 2020

Version of record online: October 12, 2020

Addition: Errors introduced during final typesetting were corrected in this version. – The Editor